



Published in final edited form as:

Proc SPIE Int Soc Opt Eng. 2016 ; 9786: . doi:10.1117/12.2216588.

Dynamic tracking of prosthetic valve motion and deformation from bi-plane x-ray views: feasibility study

Charles R. Hatt^a, Martin Wagner^b, Amish N. Raval^{c,a}, and Michael A. Speidel^{b,c}

^aDept. of Biomedical Engineering, University of Wisconsin, Madison, WI, USA

^bDept. of Medical Physics, University of Wisconsin, Madison, WI, USA

^cDept. of Medicine, University of Wisconsin, Madison, WI, USA

Abstract

Transcatheter aortic valve replacement (TAVR) requires navigation and deployment of a prosthetic valve within the aortic annulus under fluoroscopic guidance. To support improved device visualization in this procedure, this study investigates the feasibility of frame-by-frame 3D reconstruction of a moving and expanding prosthetic valve structure from simultaneous bi-plane x-ray views. In the proposed method, a dynamic 3D model of the valve is used in a 2D/3D registration framework to obtain a reconstruction of the valve. For each frame, valve model parameters describing position, orientation, expansion state, and deformation are iteratively adjusted until forward projections of the model match both bi-plane views. Simulated bi-plane imaging of a valve at different signal-difference-to-noise ratio (SDNR) levels was performed to test the approach. 20 image sequences with 50 frames of valve deployment were simulated at each SDNR. The simulation achieved a target registration error (TRE) of the estimated valve model of 0.93 ± 2.6 mm (mean \pm S.D.) for the lowest SDNR of 2. For higher SDNRs (5 to 50) a TRE of 0.04 mm \pm 0.23 mm was achieved. A tabletop phantom study was then conducted using a TAVR valve. The dynamic 3D model was constructed from high resolution CT scans and a simple expansion model. TRE was 1.22 ± 0.35 mm for expansion states varying from undeployed to fully deployed, and for moderate amounts of inter-frame motion. Results indicate that it is feasible to use bi-plane imaging to recover the 3D structure of deformable catheter devices.

Keywords

image guidance; interventional cardiology; biplane x-ray; 2D/3D registration; tracking; valve

1. INTRODUCTION

Transcatheter aortic valve replacement (TAVR) has been developed as a less invasive treatment option for patients with severe aortic valve stenosis who are high risk for open chest surgery.¹ In this fluoroscopically-guided procedure, a balloon-expandable stent-supported tissue valve is carefully positioned within the left ventricular outflow tract at the level of the aortic valve annulus. The balloon is then expanded to deploy the valve. Accurate device visualization relative to the target anatomy is both highly challenging and critical to procedure success. The purpose of this study was to develop a technique for the frame-by-frame 3D reconstruction of a moving and expanding prosthetic valve from simultaneous bi-

plane x-ray views. The method is intended for use in an interventional 3D display that portrays the valve structure registered to live 3D echo, intraprocedural CT, or pre-procedure CT/MRI.

Recently, fast 2D/3D registration algorithms for known, static objects have been reported. These algorithms determine the 3D position and orientation (“pose”) of the known object by comparison of the 2D forward projection of the 3D object model with the measured 2D x-ray image. The pose of the 3D object model is iteratively adjusted until the similarity is maximized. For example, a recently commercialized x-ray fluoroscopy/echo image fusion system relies on pose estimation of a transesophageal echocardiography (TEE) probe in order to register live x-ray and echo images.² TEE probe pose estimation at up to 92 frame/s has been reported.³

The present work adapts the 2D/3D registration framework to the case of a dynamic device which changes shape as it is deployed. In this framework, both the pose and the shape of the device are recovered from two views. Although this is an underdetermined problem for an arbitrary unknown object, for expandable devices such as a prosthetic valve, the initial device shape is known and the shape tends to change in smooth and predictable ways during deployment. It was hypothesized that by incorporation of shape constraints and a limited set of parameters describing device expansion, an accurate 3D representation could be obtained. The feasibility of the technique was investigated in simulations and in a phantom study.

2. METHODS

2.1 Dynamic pose estimation algorithm

Valve pose estimation (Figure 1) is accomplished by comparing numerical forward projections of a deformable 3D valve model to the measured 2D x-ray image(s). The valve model captures the 3D structure of the valve in different states of expansion using a limited set of adjustable parameters. (The model is established in advance, through study of the device behavior.) For each frame period, the valve model position, orientation, and shape parameters are iteratively adjusted until the similarity between the forward projection and x-ray image is maximized. Similar to rigid object tracking, where small frame-to-frame object displacements allow optimization-based methods to find the new pose of an object based on the pose from the prior frame, the current deformation at each frame is estimated using the deformation result obtained from the previous frame. An initial pose–estimate of the undeployed prosthetic valve is required for the first frame, which can either be manually provided⁴ or estimated using computer vision methods⁵.

For computational efficiency, the valve is modeled as a 3D point cloud. A simple cost function is minimized:

$$F_C = \sum_n \sum_j I_n(\vec{u}_{j,n}) = \sum_n \sum_j I_n(P_n T_n T_{\Phi} D(\vec{x}_j, \vec{m})) \quad (1)$$

$I_n(\cdot)$ is the measured x-ray image from the n th C-arm ($n = 2$ for bi-plane x-ray) and $u_{j,n}$ is the 2D position in I_n that the j^{th} 3D model point projects to. P_n is the 3D-to-2D projection matrix defining the geometry of the n th C-arm, T_n is the matrix defining the rigid transform of the n th C-arm, and T_ϕ is the matrix defining the rigid transform of the valve according to the parameters Φ (3 translational degrees of freedom and 3 rotational degrees of freedom). Finally, $D(\cdot)$ is a vector-valued function that deforms a 3D point x_j on the valve model according to the shape parameters stored in vector m . The values stored in Φ and m are adjusted during minimization. Equation (1) assumes a device with dark, discrete features on a bright background. Minimization of Eq. (1) is conceptually similar to projecting the model points onto these dark features.

2.2. Simulation study

The feasibility of the algorithm was evaluated in a simulation study where the underlying valve geometry could be exactly known. A numerical model of a valve structure was constructed from 3D sinusoidal curves wrapped around a cylinder, as shown in Figure 2. The width of the wires in the 3D model was 0.5 mm. The valve was modeled as a point cloud capable of undergoing radial expansion that varies along the long axis. The total length of the “struts” was conserved during valve expansion.

It was observed from clinical datasets that, during deployment, the valve typically starts off shaped as a cylinder with diameter W_0 , expands into the shape of a truncated cone, and finishes as a wider, shorter cylinder. Based on this observation, the deformation was parameterized with an incremental change in diameter d , as well as an additional deformation component that varied along the central axis (y-axis) of the valve (Fig 2). In this work the deformation component, d , was assumed to vary linearly with distance y along the valve axis, and therefore was parameterized by a slope s , such that $d = sy$. The distance of each model point from the central axis of the valve is $(W_0 + d)/2 + sy$. Thus the expansion behavior was described by two parameters, d and s (i.e. $m = [d \ s]$).

Digitally reconstructed radiographs (DRRs) of the expanding valve were generated in two bi-plane views (RAO 0/CRA 0, RAO 90/CRA 0) using a “splating” method.⁶ The rate of valve expansion and deformation was adjusted to visually match TAVR procedures observed clinically. Spatially correlated noise ($\sigma = 0.53$ pixels) was added to the images to achieve varying signal-difference-to-noise ratios ($SDNR = 2, 5, 10, 20, 50$) representative of fluoro- and cine-mode imaging of an Edwards Sapien valve on a flat panel cardiac angiographic x-ray system.

A total of 20 image sequences with 50 frames of valve deployment were simulated at each noise level. To simulate motion of the prosthetic valve due to a beating heart, periodic motion was added to the model during the simulation, with 2.5 degree amplitudes for pitch and roll, a 1 degree amplitude for yaw, 1.0 mm shifts for all translations, and a period of 1 second. The s parameter started out at 0, ramped up to a random peak value during the middle of the sequence, and then ramped back down to 0 at the end.

To isolate the performance of the pose estimation algorithm itself, the same general valve model was employed during pose estimation, except that the model struts were reduced to

their 3D centerlines. The true frame-to-frame position, orientation, and expansion/deformation parameters were unknown to the pose estimation algorithm. The geometry of the two bi-plane views was assumed to be known, i.e. accurate C-arm calibration was assumed. The first frame of tracking was initialized with the known ground truth. (Initialization uncertainty is investigated in Sec 2.3.)

To measure accuracy, target registration error (TRE) was computed at each frame. TRE was defined as the root mean square distance between the true locations of a set of N points on the valve model (which was perfectly known for each simulation) and the estimated locations of the same points using the dynamic pose-estimation algorithm:

$$TRE = \sqrt{\frac{\sum_{i=1}^N \left\| \vec{p}_i^{true} - \vec{p}_i^{estimated} \right\|_2^2}{N}} \quad (2)$$

2.3 Phantom study

A table-top phantom study was conducted to examine algorithm performance with an actual balloon-expandable TAVR valve. A SAPIEN XT 26 mm valve (Edwards Lifesciences Corp., Irvine, CA) was crimped on a guidewire and balloon deployment system and placed in a water bath (Figure 3). The phantom was imaged with a bi-plane x-ray angiographic system (Artis Zee, Siemens Healthcare AG, Forchheim, Germany). To collect data necessary for construction of a dynamic 3D device model, the valve was first imaged in a high-resolution cone-beam CT (CBCT) mode with an isotropic voxel size of 0.06 mm. Scans were performed in 10 different states of expansion, ranging from undeployed to fully deployed. An example 3D reconstruction is shown in Figure 4A. Based on these scans, a 3D model was designed. As shown in Figure 4B, the model was built from tubes and cuboids. Each part was converted to a 3D point cloud.

After creation of the device model, a second imaging study was performed to test the dynamic pose estimation algorithm. To establish the true 3D geometry of the valve, a standard-resolution rotational acquisition was performed with the A-plane (260° range, step size 0.85°, 100 kV, 123 mA, 2×2 Binning, 1240×960 pixel, pixel size 0.308 × 0.308 mm). CBCT reconstruction was performed with an isotropic voxel size of 0.14 mm. Scans were performed after expanding the valve to 10 different states ranging from undeployed to fully deployed. For pose estimation experiments, two x-ray projection images at -123.4 deg and -33.3 deg from each rotational 3D scan were used to represent biplane acquisition with orthogonal gantry positions. The 3D-to-2D projection matrices for both angles were extracted from the system calibration used for the CBCT reconstruction. This strategy avoided the need for B-plane calibration, which was beyond the scope of the present study, and had the added advantage that the 3D pose estimation results were automatically registered to the coordinate system of the ground truth CBCT.

The dynamic pose estimation algorithm was applied to the two selected views for each state of expansion. Since the valve's position and shape for a given expansion state did not change experimentally, the uncertainty due to frame-to-frame motion was simulated by modifying

the initial guess used in the pose estimation algorithm. The true position, which was estimated from the CBCT reconstructions, was altered by random motion vectors changing translation, rotation and the expansion of the valve at the top and bottom separately. For each expansion state, 10 different initializations were simulated.

We note that in its original form, the dynamic pose estimation allows the valve model to freely expand or contract from frame to frame. However in practice, outward expansion is much more likely. To incorporate this prior knowledge, a “penalized” cost function was also investigated. The cost function was modified to penalize device radii \hat{r}_t and \hat{r}_b at the top and bottom respectively that are smaller than the radii r_t and r_b used in the previous frame (or initialization). The following term was added to the final cost function:

$$c_r = \max(0, r_t - \hat{r}_t)^2 + \max(0, r_b - \hat{r}_b)^2 \quad (3)$$

For either pose estimation approach, TRE was calculated using manually identified point correspondences between the pose-estimated 3D model and the ground truth CBCT. Point correspondences were located at 9 outside edges on the top and bottom of the device, as shown in Figure 4C.

3. RESULTS

3.1 Simulation study

Figure 5 shows two simulated bi-plane x-ray views of the valve and the corresponding 3D reconstruction of the valve, in comparison to the ground truth, for an image frame with $\text{SDNR} = 5$. The target registration error (TRE) for each frame period was calculated as the root-mean-squared difference between the corresponding true and pose-estimated positions of all points representing peaks and valleys on the sine curves used to model the valve. Histograms of the TREs per frame for each noise level are shown in Figure 6 along with the median and the 90th percentile values.

In simulations with the lowest SDNR of 2, the target registration error (TRE) of the pose-estimated valve model was 0.93 ± 2.6 mm. For all higher SDNRs (5 to 50) an average TRE of less than 0.04 mm with a standard deviation of less than 0.23 mm was achieved. The estimated state of the valve deployment was also evaluated in terms of the difference between the estimated valve radius and the ground truth. The results showed a mean radius error of 0.30 ± 1.4 mm for $\text{SDNR} = 2$. For all higher SDNRs, mean radius error was within 0.01 ± 0.02 mm.

3.2 Phantom study

Figure 7 compares the TRE results for the phantom study using the original algorithm and the modified version which penalized valve contraction. Motion between adjacent frames was simulated for randomly oriented 3D translation vectors with magnitudes of 1, 2, and 4 mm, random Euler angle rotations of 1°, 2°, and 4°, and valve diameter changes up to 1 mm. These scenarios were selected to cover a range of expected respiratory, cardiac, and valve motions. The TRE histograms in Fig. 7 pool the TRE results for all 10 expansion states, for

a given motion magnitude, since major differences among expansion states were not observed. An example of the reconstructed 3D model compared with the reference CT is shown in Figure 8.

The original algorithm achieved a TRE of 1.22 ± 0.35 mm for the frame-to-frame motion scenarios of 1 mm translation/ 1° rotation, and 2 mm translation/ 2° rotation. The center of the device was estimated with an accuracy of 0.44 ± 0.31 mm, the radius at the center with an accuracy of 0.14 ± 0.10 mm and the rotation of the valve was determined up to an accuracy of $2.68 \pm 1.62^\circ$. For the largest motion scenarios (4 mm translation, 4° rotation, 0.5-1 mm diameter change) a TRE of 8.91 ± 17.55 mm was measured with the original algorithm compared to 4.11 ± 3.77 mm using the penalized version. Improvements observed with the penalized version were due to a reduction in the number of outlier results.

The TRE associated with the first frame of an imaging sequence was estimated separately. In this scenario, it was assumed that the valve would be in its undeployed state, and that a previously reported TAVR valve detection algorithm would provide an estimated position of the valve to within 2 mm translation and 8° rotation.[7] For this scenario, the TRE was 0.81 ± 0.00 mm.

In the two bi-plane view angles selected for analysis, the acquired images exhibited fairly homogeneous background. However due to the cuboid shape of the water bath phantom, in some view angles there were high background intensity variations which exceeded the contrast of the device structures. It was found that such variations can lead to a false positive detection of the valve in the darker areas, as shown in Figure 9. A similar effect was observed for other high contrast features in the image volume. In particular, the valve device was positioned over a guidewire with two radioopaque markers. Figure 10 shows a case where the tracking algorithm falsely identified the guidewire as part of the valve. This finding calls attention to the importance of modeling all features of the catheter device. To demonstrate potential improvements that may be achieved, the tracking algorithm was modified to exclude the guidewire from the optimization. A segmentation was performed based on the 3D acquisition to create a binary volume of the guidewire and markers. The binary volume was then forward projected into the image space and used as a mask. As shown in Figure 10D, the valve pose estimate was significantly improved by this modification.

4. DISCUSSION

This work presents a novel method for the frame-by-frame estimation of the 3D structure of a moving, expanding, and deforming catheter device from bi-plane x-ray imaging. A 3D representation of the device registered to live 3D echocardiography or pre-acquired CT/MRI models may improve image guidance in structural heart interventions where conventional 2D fluoroscopy is ambiguous. The dynamic 3D visualization is expected to yield information on the interaction between device and patient anatomy that cannot be obtained from a simple static, post-deployment visualization. This could inform investigations of clinical complications such as paravalvular regurgitation and annular rupture, and could, in turn, lead to improvements in device design. The balloon-expandable valve selected for this

initial feasibility study is currently the most commonly deployed valve design. However, these techniques could also be applied to emerging designs such as a self-expanding repositionable valve.

Simulation and phantom studies indicate the proposed method is feasible. In simulations of a moving, expanding valve device where the image SDNR was 5 or greater, the TRE averaged less than 0.04 mm, with a standard deviation of less than 0.23 mm. The simulations established the accuracy of the pose estimation procedure itself, although it should be noted that the possible modes of valve deformation were known in advance. In contrast, the phantom study performed with an actual TAVR valve required the establishment of a dynamic 3D model. In this study, the model was built from CT scans of the valve at various states of expansion and application of a simple 2-parameter deformation behavior. This first effort yielded good accuracy, with TRE of 1.22 ± 0.35 mm for expansion states varying from undeployed to fully deployed, and for moderate amounts of inter-frame motion.

Results demonstrate the importance of establishing a dynamic 3D model that precisely captures the device features and possible modes of expansion/deformation. In this study, repeated crimping and re-expanding the TAVR valve led to a slight flaring of the valve ends which was not part of our deformation model, leading to mismatches of approximately 1 mm (see Fig. 8). Clinically, similar deformation may occur if the aortic annulus is stiff and impedes balloon expansion. Incorporation of more complex deformation characteristics is expected to both improve TRE and reduce outlier results. In future work, finite element analysis based simulations of valve deformation may be used to build a statistical deformation model⁷ of the prosthetic valve, which may be able to capture the remaining degrees of deformation needed. Likewise, inclusion of features such as the guidewire and wire markers would be desirable. Future work will also investigate valve detection for the purposes of algorithm initialization,⁵ the formulation of cost functions which are robust to background intensity variations, intraprocedural C-arm calibration procedures,⁸ and, ultimately, real-time implementation of the pose estimation algorithm.

5. CONCLUSIONS

Recovery of the 3D structure of a moving and expanding valve-like structure from bi-plane x-ray views is feasible. Future work will focus on development of more realistic dynamic models for valve devices, bi-plane C-arm calibration, and development of an efficient implementation suitable for real-time display.

ACKNOWLEDGEMENTS

Research reported in this publication was supported by the National Heart, Lung, and Blood Institute of the National Institutes of Health under award numbers R01HL116567 and R01HL084022. The content is solely the responsibility of the authors and does not necessarily represent the official views of the National Institutes of Health.

REFERENCES

- [1]. Génèreux P, Head SJ, Wood DA, Kodali SK, Williams MR, Paradis JM, Spaziano M, Kappetein AP, Webb JG, Cribier A, Leon MB. Transcatheter aortic valve implantation 10-year anniversary:

- review of current evidence and clinical implications. *Eur Heart J.* 2012; 33:2388–2398. [PubMed: 22851654]
- [2]. Housden RJ, Arujuna A, Ma Y, Nijhof N, Gijsbers G, Bullens R, O'Neill M, Cooklin M, Rinaldi CA, Gill J, Kapetanakis S, Hancock J, Thomas M, Razavi R, Rhode KS. Evaluation of a real-time hybrid three-dimensional echo and x-ray imaging system for guidance of cardiac catheterisation procedures. *Medical Image Computing and Computer-Assisted Intervention--MICCAI.* 2012; 2012:25–32.
- [3]. Hatt CR, Speidel MA, Raval AN. Robust 5DOF transesophageal echo probe tracking at fluoroscopic frame rates. *Medical Image Computing and Computer-Assisted Intervention--MICCAI.* 2015; 2015:290–297. (2015).
- [4]. Karar ME, Merk DR, Chalopin C, Walther T, Falk V, Burgert O. Aortic valve prosthesis tracking for transapical aortic valve implantation. *Int J CARS.* 2011; 6:583–590.
- [5]. Hatt CR, Speidel MA, Raval AN. Hough Forests for real-time, automatic device localization in fluoroscopic images: Application to TAVR. *Medical Image Computing and Computer-Assisted Intervention--MICCAI.* 2015; 2015:307–314. (2015).
- [6]. Birkfellner W, Seemann R, Figl M, Hummel J, Ede C, Homolka P, Yang X, Niederer P, Bergmann H. Wobbled splatting—a fast perspective volume rendering method for simulation of x-ray images from CT. *Phys Med Biol.* 2005; 50:N73–84. [PubMed: 15843725]
- [7]. Zheng G, Ballester MAG, Styner M, Nolte L-P. Reconstruction of patient-specific 3D bone surface from 2D calibrated fluoroscopic images and point distribution model. *Medical Image Computing and Computer-Assisted Intervention--MICCAI.* 2006; 2006:25–32.
- [8]. Jain AK, Mustafa T, Zhou Y, Burdette C, Chirikjian GS, Fichtinger G. FTRAC—A robust fluoroscope tracking fiducial. *Med Phys.* 2005; 32:3185–3198. [PubMed: 16279072]

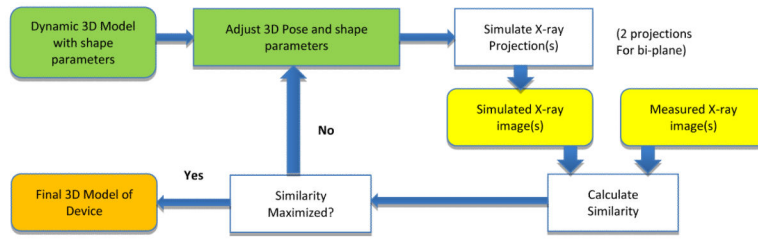


Figure 1. Flowchart of the dynamic pose estimation algorithm.

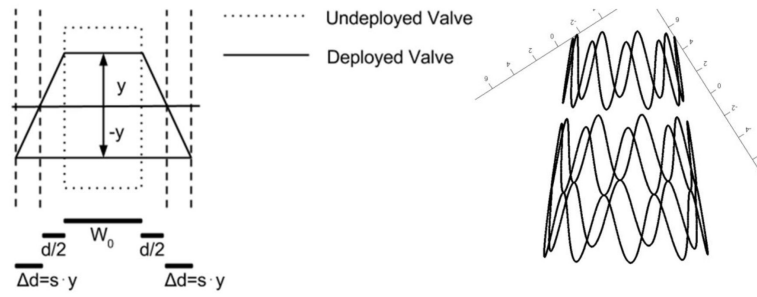


Figure 2. Left: Shape of deformable valve model. The initial undeformed state is cylindrical (dotted line). During deployment the shape is allowed to deform to a truncated cone (solid line), parameterized by d and s . Right: Side view of a partly deployed 3D model, showing the simulated valve struts.

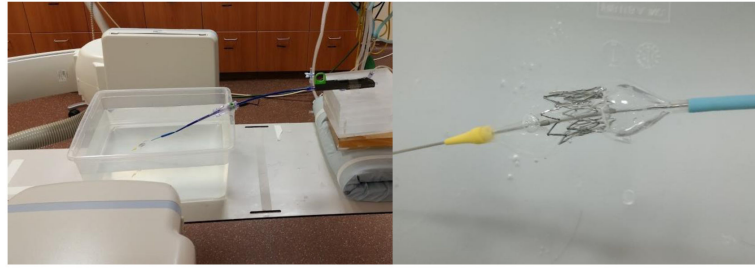


Figure 3. Left: Experimental setup for the phantom study, showing a TAVR valve stent in a water bath and the x-ray system in a lateral view. Right: Partially expanded stent with the balloon and guidewire passing through the center of the device.

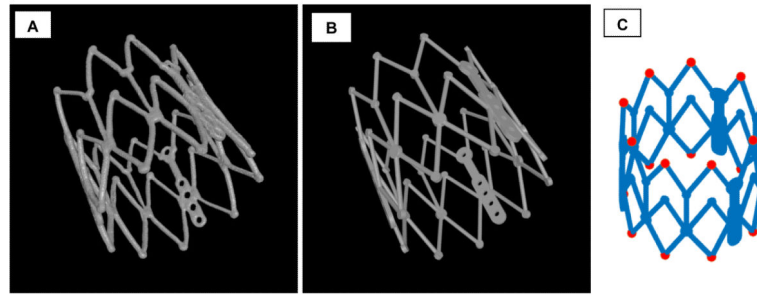


Figure 4.

A) High resolution CT scan of the TAVR valve. B) 3D model of the valve, for the same expansion state. C) In the phantom study, the apex points at the top and bottom of the valve (shown in red) were used to calculate the TRE of a pose estimate.

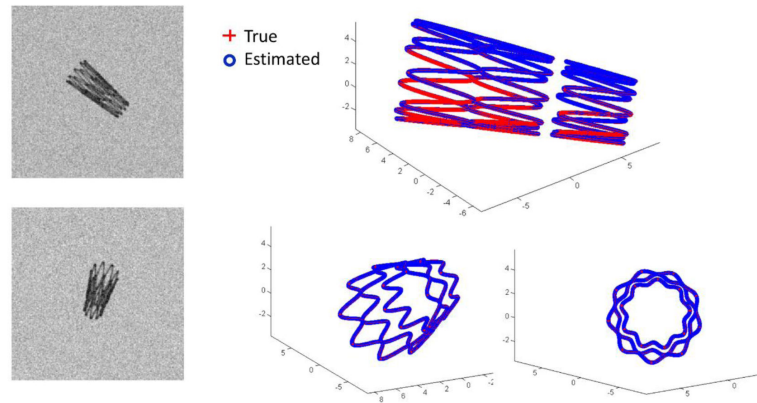


Figure 5. Example simulation results for a partially deployed valve model. Left: Simulated bi-plane x-ray projections for one frame period. Right: 3D pose-estimated (blue) and true (red) model points, shown in three different perspectives.

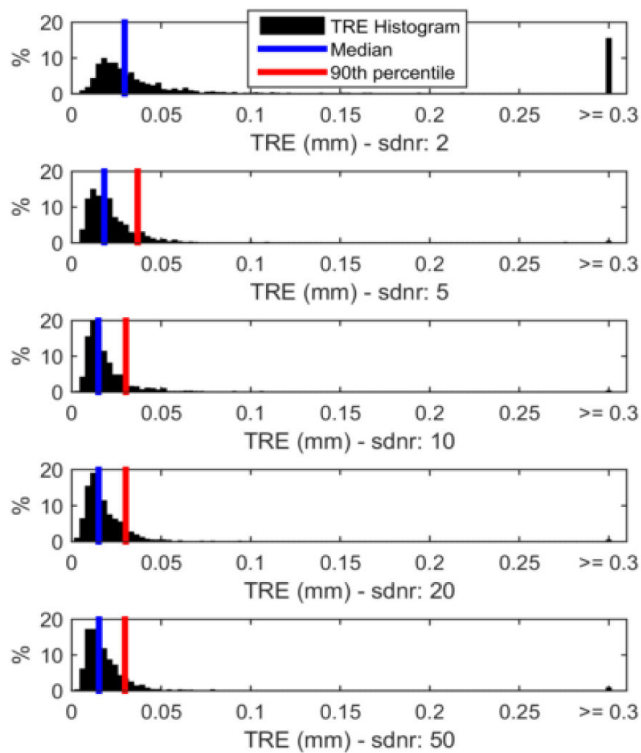


Figure 6. Tracking accuracy in simulated image sequences with SDNR = 2,5,10,20, and 50 (from top to bottom), expressed as histograms of the TRE in the individual image frames. Median TRE (blue) and 90th percentile TRE (red) are shown for each histogram.

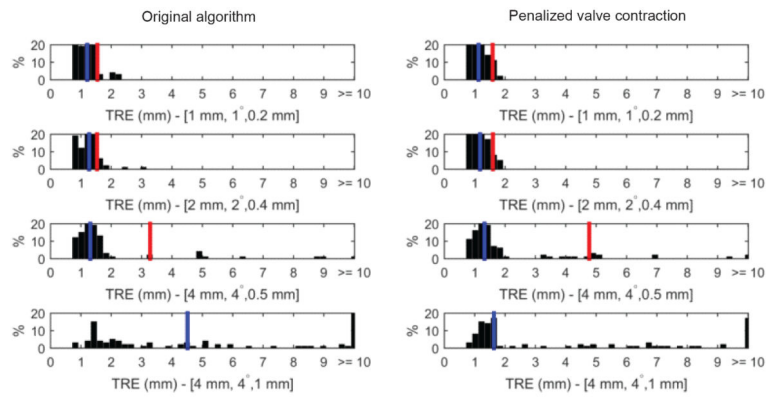


Figure 7. Tracking accuracy of the table top experiment in terms of the target registration error (TRE) for different simulated motion vectors: 1, 2, 4 and 4 mm translation in random directions, 1°, 2°, 4° and 4° rotations around arbitrary axis through the center of the device and 0.2, 0.4, 0.5 and 1 mm change of device radius randomly distributed between top and bottom. Median TRE (blue) and 90th percentile TRE (red) are shown for each histogram.

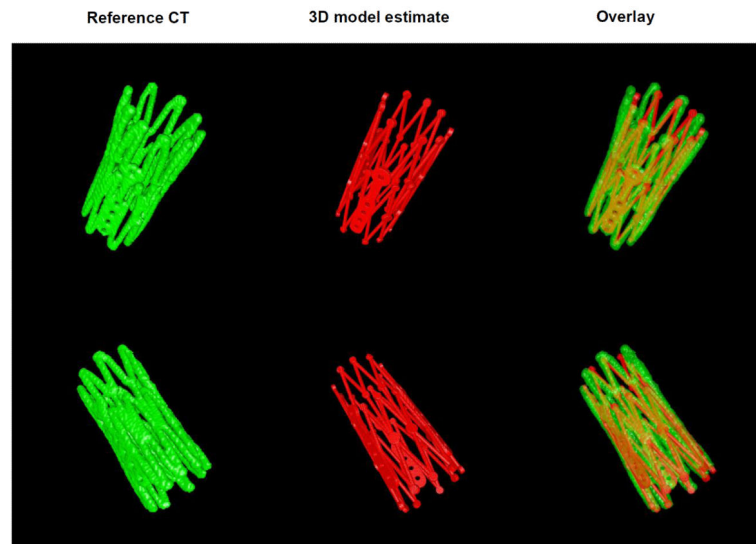


Figure 8. Example comparison of the reference CT scan of the TAVR valve (green, left column) and the 3D model derived from two x-ray views and the dynamic pose estimation (red, middle column). The top and bottom rows show the same case from two perspectives. The reference CT scan and the model estimate share the same coordinate system. Overlay is shown in the right column, using semitransparent surface rendering.

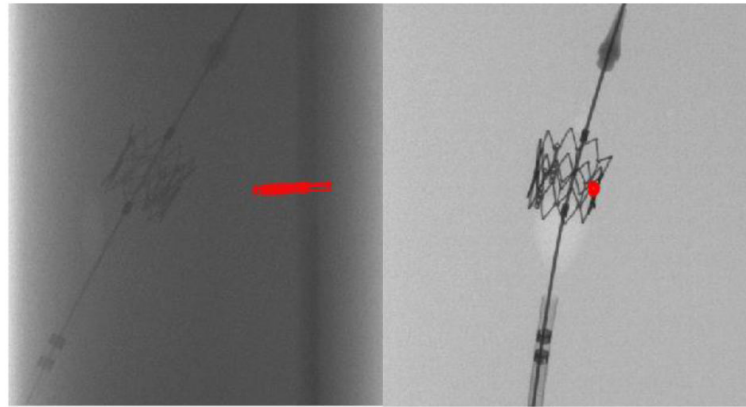


Figure 9. Case of incorrect valve tracking in the presence of a non-homogeneous background. The images are two x-ray projections acquired at 97.0° (left) and -6.9° (right) rotation angles. In this case the tracking algorithm locked onto the dark vertical feature in the left image, which was caused by the water bath geometry.

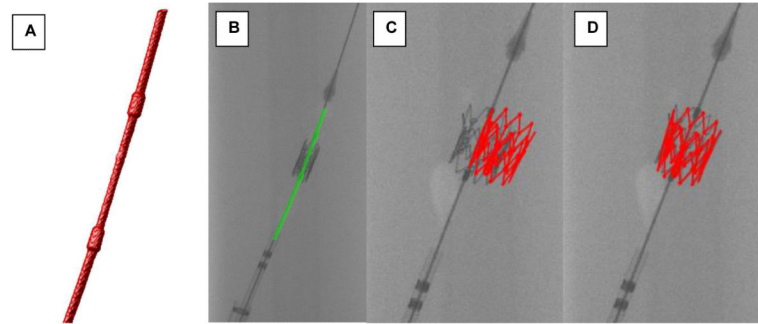


Figure 10.

A) 3D segmentation of guidewire and markers. B) Forward projection of the guidewire mask (green) overlaid with the original fluoroscopy image. C) Outlier tracking result obtained with the original algorithm. D) Result of tracking after masking out all guidewire and marker pixels.